Demonstration of power exhaust control by impurity seeding in the island divertor at Wendelstein 7-X

Florian Effenberg, Sebastijan Brezinsek, Y. Feng, M. Jakubowski, R. Koenig, M. Krychowiak, Oliver Schmitz, Y. Suzuki, D. Zhang, A. Ali, et al.

DEMONSTRATION OF POWER EXHAUST CONTROL BY IMPURITY SEEDING IN THE ISLAND DIVERTOR AT WENDELSTEIN 7-X

F. EFFENBERG[1], S. BREZINSEK[2], Y. FENG[3], M. JAKUBOWSKI[3], R. KÖNIG[3], M. KRYCHOWIAK[3], O. SCHMITZ[1], Y. SUZUKI[4], D. ZHANG[3], A. ALI[3], T. BARBUI[1], C. BIEDERMANN[3], B.D. BLACKWELL[5], G. CSEH[6], T. DITTMAR[2], P. DREWELOW[3], M. ENDLER[3], H. FRERICHS[1], Y. GAO[2], J. GEIGER[3], K. HAMMOND[3], C. KILLER[3], G. KOCSIS[6], J.D. LORE[7], H. NIEMANN[3], M. OTTE[3], A. PUIG SITJES[3], J. RUDISCHHAUSER[3], J.C. SCHMITT[8], T. SUNN PEDERSEN[3], T. SZEPESI[6], U. WENZEL[3], V. WINTERS[1] & W7-X TEAM

1 - University of Wisconsin - Madison, Madison, WI 53706, USA
2 - Forschungszentrum Jülich GmbH, 52425 Jülich, Germany
3 - Max-Planck-Institut für Plasmaphysik, 17491 Greifswald, Germany
4 - National Institute for Fusion Science, Toki 509-5292, Japan
5 - The Australian National University, Canberra, ACT 0200, Australia
6 - Wigner Research Center for Physics, H-1121, Budapest, Hungary
7 - Oak Ridge National Laboratory, Oak Ridge, TN 37830, USA
8 - Auburn University, Auburn, AL 36849, USA

Email of corresponding author: florian.effenberg@ipp.mpg.de

Abstract

Effective power exhaust by impurity seeding and its dependence on the gas species used was demonstrated in island divertor configurations for the first time at Wendelstein 7-X (W7-X). A systematic set of experiments has been conducted during the first island divertor campaign which shows that switching from neon (Ne) to nitrogen (N_2) as seeding gases enables switching from sustained to more short-pulse edge cooling. In the case of Ne seeding, significant enhancement of edge radiation with slow decay after the end of the injection is observed due to the high recycling properties of this noble gas. The N_2 seeded discharges show the response of local plasma parameters at the divertor target mostly correlated to the puff duration. Fast T_e recovery and drop of P_{rad} after the end of the puff suggest a low recycling coefficient for this impurity species. 3D modeling of these effects with EMC3-EIRENE confirms that Ne is a more effective radiator compared to N_2.

1. INTRODUCTION

The parallel heat fluxes $q_{\parallel}$ within the scrape-off layer (SOL) which are determined by the input power entering the SOL P_{SOL}, and the heat flux channel width $\lambda_{q\parallel}$, are a major concern challenging the success of next-step fusion devices. This will become crucial for the stellarator Wendelstein 7-X (W7-X), which operates inherently steady state and presently aspires to long pulse high-performance operation to demonstrate its reactor feasibility.

For tokamaks, it was found that the heat flux channel width scales with the poloidal magnetic field. Remarkable short power widths $\lambda_{q\parallel}$ in the order of a few millimeters were reported [1,2]. This usually implies an intense concentration of heat loads on divertor target tiles. The technically feasible target heat flux limits are $q_{target,max}$ $\approx$5-10 MWm^{-2} in current advanced devices. The same limits will - from the present state of knowledge - hold for ITER and DEMO [3,4], which will operate at maximum heating powers of 150 MW and 500 MW, respectively. In burning plasmas, the excess heat from the fusion reactions which enters the SOL has to be handled in addition.

To avoid damage to the PFCs (in particular for divertors with metal target plate materials) due to excessive heat fluxes and material erosion, additional means to control and mitigate the heat flux issue are under investigation. Radiative edge cooling is a promising approach to remove most of the thermal power from the main plasma confinement before reaching the plasma-facing components (PFCs). Here, dedicated low and medium atomic charge impurity species are used to dissipate significant amounts of the power entering the SOL by impurity line emission. This power loss channel allows, in principle, for active control and manipulation of the energy balance mostly through the amount of impurities released into the plasma. For steady state, long pulse operation, it is desired to use the impurity line radiation to cool the plasma edge such that the temperatures downstream near the main PFCs are reduced and reliably controlled at levels of a few eV. The intrinsic impurity line radiation is determined by the wall material and sputtering physics. Impurity seeding will remain the only means for active control of the radiative power losses in the plasma edge in the case of persistent high Z materials. Multiple

studies of radiative power exhaust, including impurity seeding, have been conducted at the tokamaks TEXTOR, ASDEX-U, JET, and ALCATOR C-MOD [6-14] and the LHD stellarator [15-18].

For long pulse high-performance operation, it is desired to achieve and sustain divertor conditions with low temperatures, high densities, and good neutral pumping and heat fluxes at the targets below the technically critical limits. An ideal regime is the so-called 'detached divertor' regime [19] which is also characterized by enhanced radiation and reduced recycling fluxes. The main fraction of the parallel heat flux is dissipated in the high density, recombining plasma in front of the plates in this regime. Detachment in tokamaks requires recombining plasmas at electron temperatures of Te<1 eV in the divertor. The stellarator, however, promises the feasibility of power detachment at higher temperatures (10 eV) due to increased momentum losses by counter-streaming flows [20]. The friction between these flows can induce significant pressure drops without intensive ion-neutral collisions. This enables stable operation at low heat fluxes with still substantial but cold particle fluxes. This combination allows for good neutral exhaust during the detachment and might be a unique regime for volumetric divertors like the island divertor under investigation at W7-X. Impurity radiation strongly determines the SOL power balance in such a divertor scenario.

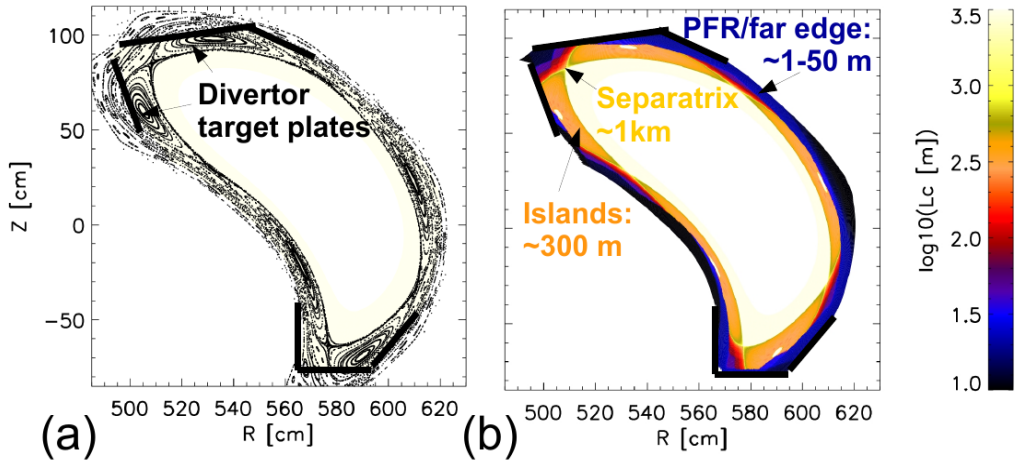

Figure 1: (a) Poincare plot of the boundary magnetic vacuum field of the standard divertor configuration. The divertor target plates (solid lines) intersect with the 5/5 magentic islands. (b) The target-to-target connection lengths Lc represent the open magnetic field lines.

The island divertor at W7-X is new territory for radiative power exhaust with impurity seeding. Development of radiative cooling as possible means for power dissipation requires, at the same time, an understanding of the basics of heat and particle transport in the island divertor topology. This has to be studied in the present situation of a carbon wall. In view of operational aspects for future fusion devices, radiative edge cooling by impurity seeding might become of critical importance. W7-X is presently fully equipped with graphite PFCs, but as a long-term goal and for a potential W7 reactor [21,22] it is planned to replace graphite PFCs and probably make use of tungsten, advanced tungsten alloys or other metallic elements as the first wall material. This means that carbon as an intrinsic radiator would be suppressed, and hence a form of self-regulated power load control by enhanced sputtering at higher temperatures which reduces the divertor temperature back to acceptable values, is lost. Impurity seeding will be the only means for power dissipation in the edge to achieve detached operation. Therefore it is crucial to investigate impurity seeding, transport, and the related PSI physics in the 3D environment of current stellarators.

The purpose of this study is to explore if and how actively injected radiator gases can aid in cooling the island divertor plasma and eventually allow to achieve and control detachment. This study contributes to the high-level requirements for a next-step stellarator toward a HELIAS power plant as specified in [22].

2. GEOMETRIC PROPERTIES OF THE ISLAND DIVERTOR CONFIGURATION

A Poincare plot of the vacuum magnetic field line structure of the W7-X island divertor configuration at a toroidal cross section (ϕ=12.3º) is shown in figure 1 (a). Five main resonances are visible as sub-confinement structures in the boundary. These five independent magnetic islands are a characteristic feature of all ι(a)=5/5 configurations. These 5/5 islands intersect with the divertor plates (solid black lines). The resulting SOL is defined by the open field lines. These field lines are shown in the target-to-target connection lengths (L_C) distributions in figure 1 (b) in a logarithmic representation. The separatrix, which distinguishes the island domain from the closed flux surface domain of the plasma core, consists of open field lines of lengths of lengths O(1 km) (yellow → white). The island consists of L_C~O(100 m)(orange). In the far SOL, deep in the divertor shadows and near the pumping gaps (remote volume beyond the island X-points), the connection lengths are O(1 m)-O(10 m) (black → blue). This outer domain is regarding the length scale similar to the initial limiter configuration or typical tokamak configurations.

Inside the islands, a region exists in which the divertor target plates do not intersect the island flux surfaces. These regions are the O-points or magnetic axis of the islands. Error field correction is usually required in order to bring the islands into their nominal position [23,24]. The typical parallel transport length scale in the island divertor is L_C~200 m. During the longer parallel path toward the targets, cross-field transport can be more effective compared to limiter or tokamak configurations due to the longer path lengths on which radial diffusion can occur (e.g., λ_n~$L_C^{0.5}$). The island divertor obeys, in general, a larger perpendicular to parallel transport ratio for heat and particles [20].

Within the SOL, which mostly consists of the magnetic islands, heat and particles are guided within the fast parallel transport channels along open field lines towards the divertor targets, also known as downstream location. During the relatively long parallel transport, heat and particles may also perform further cross-field diffusion within the SOL. In contrast to configurations with closed magnetic flux surfaces, the effective perpendicular transport within the island SOL does also include a component from parallel transport in the radial direction. This parallel transport in radial direction occurs because the field lines orbit around the island O-point until they hit the target. The islands create an effective radial heat and particle loss channel by fast parallel transport.

Since this 3D island divertor is designed to screen and exhaust impurities very efficiently, it remains an open question if it is possible to achieve at the same time substantial radiative power exhaust by local impurity injection.

3. RADIATIVE POWER EXHAUST WITH IMPURITY SEEDING

Ne and N2 are chosen because their radiation potentials are peaking below 100 eV, and therefore, they are the most promising candidates within the SOL for the plasma performance achievable in the first divertor campaign. Two scenarios with neon and nitrogen seeding in the standard island divertor configuration were realized (#20171207.045 and #20171207.048). The respective impurity species were injected near the island O-point through a piezo valve of the He beam gas feed. In the following, the effects of two different coolant gases are compared in a scenario with attached conditions.

3.1 NE SEEDING: HIGH RECYCLING & SUSTAINED PRAD ENHANCEMENT

The overview of main discharge parameters of #20171207.045 is shown in figure 2 (a). The ECRH power is 2.9 MW. Feedback-controlled fueling was used to achieve a relatively stationary line averaged density of $\int n_e dl$ = $1.8 \cdot 10^{19}$ m^{-3}. The Ne injection starts at t-t_1=3 s and lasts for $\tau_{Ne,inj.}$=200 ms (indicated by dashed lines in figure 2 (a)). The Ne flux rate was Γ_{Ne}=$5 \cdot 10^{19}$ atoms/s. The line averaged density increases slightly by 10% in response to the seeding. The energy confinement is not degraded (ΔW_{dia}~0, $\Delta \tau_E$~0) despite the significant enhancement of total radiation.

The time evolution of Prad measured with the bolometer, and the divertor heat flux profiles on the horizontal divertor targets measured by IR cameras are compared in figure 2 (b) (top and bottom). The radiation increases by almost a factor of two. A drop of heat fluxes by 30-40% after the termination of the 400 ms Ne injection is seen. The enhanced radiation decays only slowly over seconds, and the divertor heat fluxes increase only slowly and marginally after the end of Ne injection. Neon was injected only through a single divertor gas box valve into

the island center at one toroidal location. However, a drop of heat fluxes is measured on horizontal targets connected to the seeded and the unseeded island.

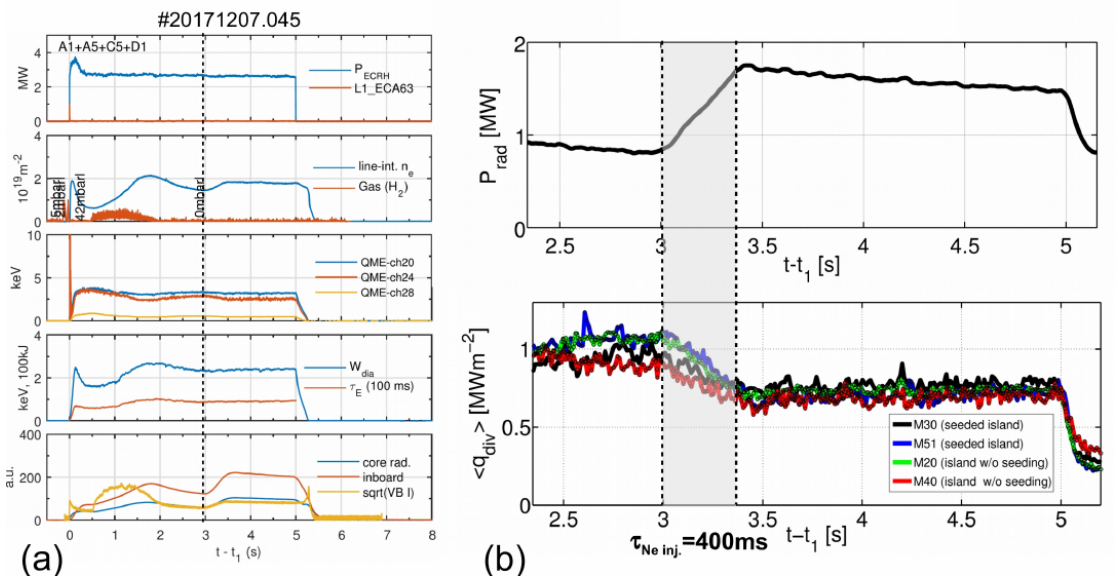

Figure 2: (a) Overview of main plasma parameter. (b) (top) total radiated power from bolometer measurement and (bottom) peak divertor heat fluxes with 400 ms Ne puff (comparing divertors connected to seeded and un-seeded islands).

3.2 N_2 SEEDING: LOWER RECYCLING ALLOWS FOR SHORT COOLING PULSES

N_2 was injected at the same location (He beam) into the island as Ne. The overview of the main plasma parameter (#20171207.048) is shown in figure 3 (a). The ECRH power was 2 MW. The line average density $\int n_e dl = 1.6 \cdot 10^{19}$ m^{-2}. Nitrogen is injected at t-t_1=3 s for 270 ms and t-t_1=4.5 s for 500 ms (indicated by dashed lines). The nitrogen particle flux rate is $\Gamma_{N2} \sim 2 \cdot 10^{20}$ s^{-1}.

The line averaged density is increased by 20% in response to the N2 injection. The edge radiation is enhanced by 40%. The energy confinement properties remain constant in response to the impurity seeding. The electron temperature T_e was measured with the Helium beam in the seeded island, and the heat fluxes on the divertors connected to the seeded island are shown in figure 3 (b) (top and bottom). The time evolution is shown for channels 1, 9, 5, and 13, which correspond to increasing radial distance from the horizontal target towards the separatrix (indicated by the arrow labeled with r_{eff}). The error bars plotted for the T_e measurements are total uncertainties, which include the actual measurement uncertainty in the order of 5-8 eV and the systematic uncertainty from the collisional-radiative model used for the analysis of the line ratio values measured on He line emission [25].

Both T_e and $q_{div,max}$ show a drop in response to the N_2 injection, but also a relatively fast recovery almost over the same time scale as the injection time O(100 ms) in correlation with the response of P_{rad} shown in figure 2 (a). Similarly, a fast drop and recovery occurs during the second short N_2 injection t-t_1=4.5 s.

This scenario demonstrates that nitrogen allows radiative power exhaust without confinement degradation but generally features a fast recovery of plasma parameters after the termination of the puff. This agrees with measurements made during the experiments in the limiter configuration and suggests low recycling on graphite walls.

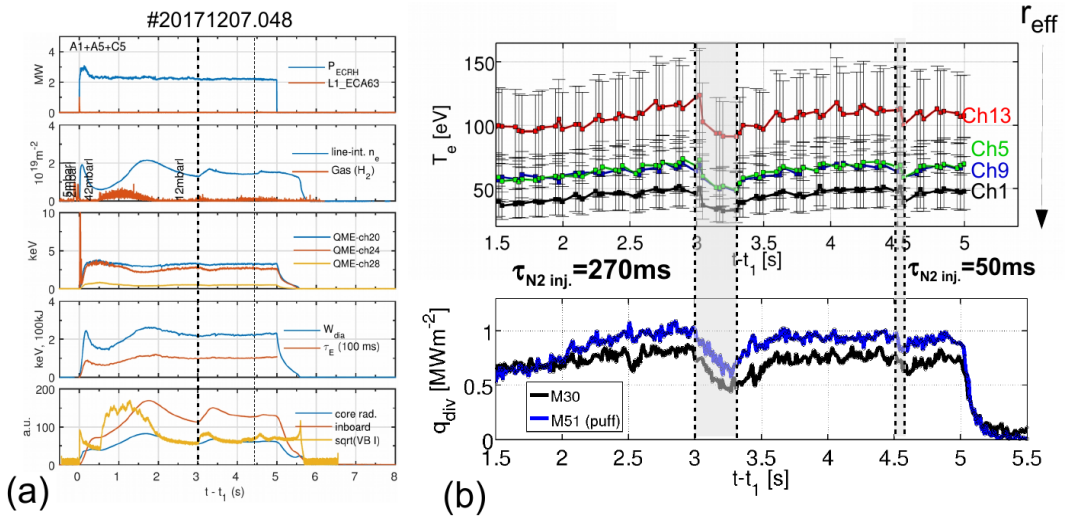

Figure 3: (a) Overview of main plasma parameter (b) (top) electron temperature measured with the He beam and (bottom) peak divertor heat fluxes measured with IR cameras. The dashed lines indicate the timing of the N_2 injections.

4 MODELING OF IMPURITY SEEDING IN THE ISLAND DIVERTOR

The 3D coupled plasma fluid and kinetic neutral edge transport Monte Carlo code EMC3-EIRENE is commonly used [26-29] for predictive modeling and the interpretation of experimental results in the domain of plasma wall interactions and SOL transport. Calculations with EMC3-EIRENE performed in the first attempt in preparation of seeding experiments assumed fixed upstream conditions of n_e~1e19 m^{-3} at an input power of 2.5 MW which may correspond to a scenario with higher heating power but anticipates power losses of intrinsic impurities. The anomalous transport coefficients were assumed to be $D_\perp$ = 0.5 m^2s^{-1} and $\chi_{\perp i,e} = 3D_\perp$. Impurity seeding in the island divertor was simulated either assuming sourcing scaled with the main recycling flux or sourced from the puff location only. Fixed power loss fractions of f_{rad}=0.4 were set according to estimations of the inboard radiation measured with the bolometer. The main results of a first comparison of the features of radiative power exhaust with Ne and N2 seeding within the modeling and its impact on divertor heat fluxes are shown in figure 4. Figure 4 (a) shows the distribution of the total radiated power in the divertor volume in the case of Ne sourced from the main recycling domain. Figure 4 (b) shows the distribution of total power losses in the case of N_2 seeding without recycling. Furthermore, Ne was treated like N_2 without recycling. In this case, the total Prad is similar to the distribution in figure 4 (b) but slightly shifted inwards. The impact of Ne and N_2 seeding with and without recycling on the main divertor heat fluxes is shown in figure 4 (c) and (d), respectively. The most substantial reduction of heat fluxes is found for Ne sourced from the main recycling region. This makes sense since, in this case, the radiative losses are concentrated downstream in the region of maximum power deposition. The heat fluxes are slightly less reduced in the case of Ne and N2 sourced from the puff location in the island center without recycling (figure 4(a, blue) and 4(b)). The heat load reduction scales roughly with the power loss fraction estimated from the inboard bolometer signal. Also, the modeling shows that almost twice as much atomic N is required to achieve the same power losses as Ne. The 3D modeling confirms the main features of the power exhaust experiments and will have to be adjusted stepwise to investigate the specific aspects of PWI and take more realistic sputtering and recycling into account.

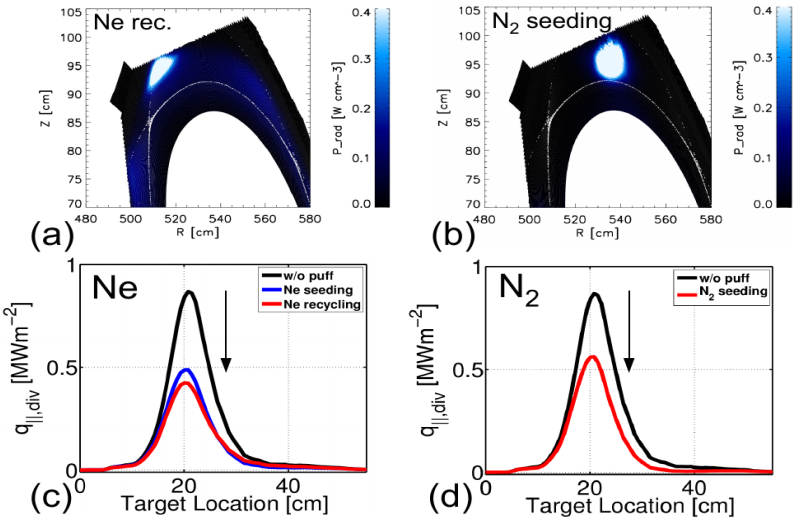

Figure 4: (a) Total P_{rad} of Ne after puff sourced proportional to recycling flux (b) Total P_{rad} of N_2 during puff neglecting recycling (c) Averaged divertor heat fluxes for Ne with (red) and without recycling (blue) (d) Averaged divertor heat fluxes in case of N_2 seeding without recycling.

5. CONCLUSIONS

Radiative power exhaust experiments with impurity seeding have been conducted for the first time in the W7-X island divertor. Two seeding gases have been investigated concerning their cooling efficiencies and recycling behavior. Ne is found to feature high recycling and thereby allows for sustained P_{rad} enhancement with slow decay over seconds. A reduction of the peak heat fluxes onto the divertors by 40-50% without degradation of energy confinement was demonstrated. In order to achieve a comparable drop in divertor heat fluxes, N_2 seeding requires a higher influx rate and allowed only for a short time Prad enhancement indicating its low recycling properties.

The comparison of neon and nitrogen seeding shows that neon is a more efficient radiator because stronger radiative exhaust can be achieved with fewer particles. This is certainly due to the higher number of energy levels of Ne atoms compared to N atoms (Z=10 vs. Z=7). Furthermore, nitrogen appears to have a lower residence time due to its low recycling on the graphite walls and therefore requires a higher influx to sustain a certain level of line emission.

The major features of seeding with Ne and N_2 have been investigated with 3D modeling. The differences in cooling efficiencies and the general effectiveness for heat flux mitigation have recovered in a first simplified attempt. Here, the number of deposited particles can be compared more directly, and the ratio is found to be $\int \Gamma_{N2} d\tau / \int \Gamma_{Ne} d\tau \sim 4$.

Both radiators suggest allowing for edge cooling and reduction of divertor heat loads without degradation of energy confinement. Effects on sputtering and cooling symmetry will be a matter of further analysis and are beyond the scope of the presented work.

ACKNOWLEDGEMENTS

This work was supported in part by the U.S. Department of Energy (DoE) under grant DE-SC0014210 and by start-up funds of the Department of Engineering Physics and of the College of Nuclear Engineering at the University of Wisconsin - Madison, USA.

This work has been carried out within the framework of the EUROfusion Consortium and has received funding from the Euratom research and training programme 2014-2018 under grant agreement No 633053. The views and opinions expressed herein do not necessarily reflect those of the European Commission.

This research was performed using the computer resources and assistance of the UW-Madison Center For High Throughput Computing (CHTC) and the high performance computing systems ”Hydra” and ”Draco” of the Max-Planck-Gesellschaft at Rechenzentrum Garching (RZG).

REFERENCES

[1] EICH, T. et al., Phys. Rev. Lett., **107**:215001, Nov 2011
[2] GOLDSTON, R.J., Nuclear Fusion, **52**(1):013009, 2012
[3] ZOHM, H. et al., Nuclear Fusion, **53**(7):073019, 2013
[4] FEDERICI, G. et al., Fusion Engineering and Design, **89**(7):882 – 889, 2014
[5] SAMM, U. et al., Plasma Physics and Controlled Fusion, **35**(SB):B167, 1993
[6] MESSIAEN, A.M. et al., Nuclear Fusion, **34**(6):825, 1994
[7] G. TELESCA, G. et al., Journal of Nuclear Materials, **241**-**243**:853–856, 1997
[8] RAPP, J. et al., Nuclear Fusion, **44**(2):312, 2004
[9] KALLENBACH, A. et al., Journal of Nuclear Materials, **415**(1, Supplement):S19 – S26, 2011
[10] KALLENBACH, A. et al., Plasma Physics and Controlled Fusion, **55**(12):124041, 2013.
[11] REINKE M.L., et al., Journal of Nuclear Materials, **415**(1, Supplement):S340 – S344, 2011
[12] MADDISON, G.P., et al., Nuclear Fusion, **51**(4):042001, 2011
[13] LORE, J.D., et al., Physics of Plasmas, **22**(5):056106, 2015
[14] BERNERT, M., et al., Nuclear Materials and Energy, **12**:111–118, 2017
[15] KOBAYASHI, M., et al., Nuclear Fusion, **53**(9):093032, 2013
[16] MUKAI, K., et al., Nuclear Fusion, **55**(8):083016, 2015
[17] MORISAKI, T., et al., Journal of Nuclear Materials, **463**:640 – 643, 2015
[18] TANAKA, H. et al., Nuclear Materials and Energy, **12**:241 – 246, 2017
[19] MATTHEWS, G.F. Journal of Nuclear Materials, **220**-**222**:104 – 116, 1995
[20] FENG, Y. et al., Nuclear Fusion, **46**(8):807, 2006.
[21] FENG, Y., Journal of Nuclear Materials, **438**, Supplement:S497 – S500, 2013
[22] WARMER, F., et al., Plasma Physics and Controlled Fusion, **58**(7):074006, 2016
[23] OTTE, M., et al, 2016 Plasma Phys. Control. Fusion **58** 064003
[24] BOZHENKOV, S.A. et al, 2017 Nucl. Fusion **57** 126030
[25] SCHMITZ, O., et al., Plasma Physics and Controlled Fusion, **50**(11):115004, 2008
[26] BADER, A. et al., Nuclear Fusion, **53**(11):113036, 2013
[27] KOBAYASHI, M, et al., Nuclear Fusion, **55**(10):104021, 2015
[28] SAHOO, B.P. et al., Physics of Plasmas, **24**(8):082505, 2017
[29] MARCINKO, S. and CURRELI, D., Physics of Plasmas, **25**(2):022507, 2018